A superoxide dismutase mimic nanocomposite for amperometric sensing of superoxide anions

ARTICLE *in* MICROCHIMICA ACTA · DECEMBER 2014

Impact Factor: 3.74 · DOI: 10.1007/s00604-014-1424-1

4 AUTHORS, INCLUDING:

Fariba Dashtestani

University of Tehran

8 PUBLICATIONS **17** CITATIONS

SEE PROFILE

Hedayatollah Ghourchian

University of Tehran

113 PUBLICATIONS **802** CITATIONS

SEE PROFILE

Khadijeh Eskandari

University of Tehran

18 PUBLICATIONS **89** CITATIONS

SEE PROFILE

Microchim Acta
DOI 10.1007/s00604-014-1424-1

ORIGINAL PAPER

A superoxide dismutase mimic nanocomposite for amperometric sensing of superoxide anions

Fariba Dashtestani · Hedayatollah Ghourchian · Khadijeh Eskandari · Hossain-Ali Rafiee-Pour

Received: 30 August 2014 / Accepted: 19 November 2014

Abstract A nanocomposite consisting of gold nanoparticles and the copper(II) complex of cysteine (GNP/Cu-Cys) is shown to represent a useful mimic for the enzyme superoxide dismutase (SOD). The relative activities of plain GNPs, Cu metal, Cys, Cu-Cys and GNP/Cu-Cys were determined and compared to those of native SOD. The value for half-maximal inhibitory concentration of the nanocomposite is 0.3 μg mL^{-1} which is 3 times higher than that of the native enzyme. The GNPs/Cu-Cys nanocomposite was immobilized on a carbon paste electrode and used as a biomimetic sensor for the detection of superoxide anions. The resulting sensor has a linear range over the concentration range from 3.1 to 326 μM, a detection limit of 2.8 μM (at an S/N of 3), and a sensitivity of 0.018 μA μM.cm^{-2}. The selectivity for superoxide anions over potential interferents such as hydrogen peroxide, uric acid and citric acid is excellent.

Keywords Superoxide dismutase mimic · Biomimetic sensor · Cysteine · Gold nanoparticles

Electronic supplementary material The online version of this article (doi:10.1007/s00604-014-1424-1) contains supplementary material, which is available to authorized users.

F. Dashtestani · H. Ghourchian (✉)
Laboratory of Microanalysis, Institute of Biochemistry & Biophysics, University of Tehran, P.O. Box 13145-1384, Tehran, I.R. Iran
e-mail: hadi@ibb.ut.ac.ir

K. Eskandari
Nanobiotechnology Research Center, Baqiatallah University of Medical Sciences, Tehran, I.R. Iran

H.-A. Rafiee-Pour
Biotechnology Division, Department of Molecular and Cell Biology, Faculty of Chemistry, University of Kashan, P. O. Box, 78317-51167, Kashan, I.R. Iran

Introduction

Superoxide radical anion ($O_2^{\bullet-}$) is generated during cellular metabolism in aerobic organisms. $O_2^{\bullet-}$ may initiate a series of free radical reactions that may result in diseases such as stroke, cancer, inflammatory disorders, oxidative stress and so on [1]. Superoxide dismutase (SOD) represents an essential defense system to detoxify $O_2^{\bullet-}$ in living organisms. SODs are a class of oxidoreductase enzymes which contain Cu-Zn, Mn, Fe or Ni in the active site. They catalyze the dismutation of $O_2^{\bullet-}$ to molecular dioxygen (O_2) and hydrogen peroxide (H_2O_2) via a cyclic oxidation–reduction electron transfer mechanism [2] and as a result scavenge the $O_2^{\bullet-}$ activity.

However, it has been reported that in many diseases, SOD is suppressed by $O_2^{\bullet-}$ [3]. In such cases it is necessary the SOD to be provided from outside. However, applying natural SOD is limited due to its high cost, and also some troubles in its oral treatment, chemical stability, cell permeability and immunogenicity [4]. To overcome these limitations, much effort has been made in developing new SOD mimetics compounds for a wide range of biomedical and technological applications [5] such as biomimetic sensors for detection of $O_2^{\bullet-}$ [6].

SOD mimetics compounds which are active and selective and also more stable and economic than natural SOD has attracted much attention. Most of these compounds, being developed so far, were based on manganese, cupric and ferric complexes with chelators such as porphyrins [7], macrocyclics [8, 9], schiff-bases [10], imidazoles [11] and amino acids derivatives [12]. In our recently published report we realized that the cupric ions which coordinated to cysteine and immobilized on gold electrode represents specificity to $O_2^{\bullet-}$ [13]. So, it was concluded that copper cysteine complex could act as a SOD mimic enzyme and might serve as a good $O_2^{\bullet-}$ scavenger.

Published online: 02 December 2014

Nowadays, the research on intrinsic enzyme-like activity of nanoparticles (NPs) has become a growing area of interest. It has been reported that ceria nanoparticles [14], pectin-coated GNPs, gold-platinum nano-alloy particles [15] and platinum NPs [16, 17] exhibited SOD like activity. NPs have demonstrated significant catalytic activity because of their high surface-to-volume ratio [18]. This makes efficient exposure of NPs to reagents in solution and enhances their catalytic activity [19]. Among the noble metals, gold nanoparticles (GNPs) have received great attention in this regard. GNPs display the electronic properties which allow them to capture/release electrons in redox reactions so that they are commonly used as redox mediators in electrochemical biosensors [20–22].

An interesting challenge in nanocatalysts is to gain metal nanoparticles capped with metal complexes which could mimic metalloenzymes [23]. In this sense, by capping gold nanoparticles on copper-cysteine (Cu-Cys) complex [13], a novel nanocomposite (gold/copper-cysteine, GNPs/Cu-Cys) was developed which shows SOD mimetic activity. Then, the SOD mimetic activity of the nanocomposite against $O_2^{\bullet-}$ was investigated using carbon paste electrode (CP) and UV–vis spectroscopy.

Experimental

Materials and methods

Materials

Pyrogallol, tris-hydroxymethyl aminomethane buffer (Tris), ethylene-diamine-tetra acetic acid (EDTA), hydrochloric acid, carbon graphite powder, paraffin oil, hydrogen tetracholoroaurate ($HAuCl_4.3H_2O$), trisodium citrate, potassium superoxide (KO_2), dimethyl sulfoxide (DMSO), potassium phosphate buffer and copper acetate were purchased from Merck (www. Merck.com). L-cysteine was purchased from Sigma-Aldrich (www.sigmaaldrich.com). The potassium phosphate buffer (0.02 M) were prepared by mixing of KH_2PO_4 and K_2HPO_4 and adjusting the pH to 7.4.

$O_2^{\bullet-}$ standard samples

A stock solution of $O_2^{\bullet-}$ was prepared by adding 1 mg KO_2 to 2 ml DMSO and sonication the solution for 10 min [24]. The concentration was determined by using its extinction coefficient (2686 M^{-1} cm^{-1}) at 256 nm. The concentration of the $O_2^{\bullet-}$ stock solution was determined to be 6.78 mM. The prepared solution can be used as standard for amperometric measurements of superoxide as SOD substrate.

Apparatus

The sonication was carried out using an ultrasonic bath (Techno-Gaz, Italy). Raman spectra were recorded with a SENTERRA 2009 (Bruker, Germany) spectrometer. UV–vis spectra were recorded in a Carry 100Bio spectrophotometer (Varian, Australia). Dynamic light scattering (DLS), Zeta plus (Brookhaven, USA) was used for size determination of nanoparticles. The Surface properties of the prepared particles (GNPs, Cu-Cys and GNPs/Cu-Cys) were recorded using atomic force microscopy (AFM, NTMDT, Russia) in semi contact mode through silicon tip and the images size was 2× 2 μm^2. Fourier transforms infrared spectroscopy (FT-IR) of nanoparticles in KBr disc was carried out using a Perkin-Elmer 343 spectrometer (USA). Electrochemical experiments were performed with a computer controlled m-Autolab modular electrochemical system (Eco Chemie Ultecht, The Netherlands), driven with GPES software (Eco Chemie). A conventional three-electrode cell was used with an Ag/AgCl, (saturate KCl) as reference electrode (Azar electrode, Uromia, Iran), a Pt wire (from Metrohm) as counter electrode and a homemade carbon paste electrode (Φ=2.5 mm) as working electrode. Electrochemical impedance spectroscopy (EIS) characterization was carried out in $K_3Fe(CN)_6$ (5 mM)/KCl (50 mM) as a redox probe using a PGSTAT30/FRA2 system (Autolab, Netherlands).

Preparation and characterization of nanoparticles

The Cu-Cys complex was synthesized by solvent free method [25]. Briefly, L-cysteine (0.10 g) and copper acetate (0.08 g) were mixed and ground by an agate mortar till acetic acid smell was released. After 5 h, the reaction was completed and the sky blue microcrystals were obtained by washing with methanol. The FT-IR spectrum of Cu-Cys complex in KBr disc was recorded and compared with literature.

Colloidal gold nanoparticles were prepared according to the Turkevich method [26]. Briefly, 0.5 mL of 1 % (*w/v*) sodium citrate solution was added to 50 mL of 0.01 % (w/v) $HAuCl_4 \cdot 3H_2O$ and heated up to 60 °C. The final mixture of red color was boiled for 15 min and stored in dark glass bottles at 4 °C. All glassware used in this procedure was cleaned by freshly prepared 1:3 HNO_3–HCl and rinsed thoroughly with distilled water.

For the preparation of GNPs/Cu-Cys nanocomposite 0.1 mg Cu-Cys complex dispersed in 10 mL distilled water by 10 min sonication at room temperature. Then, 1 mL colloidal GNPs was added to the Cu-Cys complex. After stirring for 4 h, the resulting nano-composite was centrifuged at 5000 rpm for 30 min to remove the unbound GNPs.

For investigation of synthesized Cu-Cys and GNPs/Cu-Cys Raman spectra were recorded. And also, DLS was used for size determination of GNPs, Cu-Cys and GNPs/Cu-Cys.

The Surface properties of the prepared particles (GNPs, Cu-Cys and GNPs/Cu-Cys) were recorded using AFM.

SOD activity assay

Superoxide was generated indirectly at alkaline pH by the action of oxygen on pyrogallol. SOD reacts with the superoxide and this slows down the formation rate of the o-hydroxy-o-benzoquinone and other polymer products. One unit of SOD is defined as the amount of enzyme that inhibits the rate of pyrogallol autoxidation by 50 % [27]. The assay was performed in 1 mL of 0.05 M Tris/HCl buffer at pH 8.2 containing 10^{-4} M EDTA at 27 °C [27]. The standard reaction mixture usually contained a certain concentration of pyrogallol, which produces an autoxidation rate of 0.07 (absorbance per minute) at 325 nm. Under this condition, the amount of SOD or its mimetic compounds that is required for decreasing the autoxidation rate of pyrogallol to 0.035 absorbance per min is defined as one unit of activity and called half-maximal inhibitory concentration (IC_{50}).

Preparation of CP modified electrodes

CP electrodes were prepared by mixing 20 mg of graphite powder with 15 μL of paraffin oil with a mortar and pestle. A modified paste was prepared in a similar method, except that the graphite powder was mixed with a desired weight of Cu-Cys complex to get different composition as given in Table 1. Both unmodified and modified pastes were packed into a polyethylene tube (inner diameter 5 mm). Electrical contact to the paste was established via inserting a copper wire thorough flank. The surface of the packed carbon paste was smoothed on paper. For preparing GNPs conjugated CP, the surface of optimized modified CP were inserted in GNPs for 4 h then, the electrode was gently rinsed with deionized water.

Results and discussion

Characterizations of GNPs/Cu-Cys nanocomposite

To characterize the synthesized GNPs, different techniques were used. UV–Vis spectroscopy showed the absorbance at 540 nm which was consistent with the data reported in the literature [28] (data not shown).

FT-IR spectroscopy has proven to be useful for recognition of the synthesized Cu-Cys. Comparison between the resulting FT-IR spectra for Cu-Cys complex in KBr disc and that obtained for free cysteine (data not shown) indicated that the thiol stretching band at 2551 cm^{-1} was missed perhaps due to the deprotonating and binding of cysteine thiol group to copper atom. In addition, the asymmetric and symmetric band of carboxylate group around 1500 cm^{-1} remained unchanged in both free cysteine and Cu-Cys complex. This indicates that the carboxylic acid in cysteine was not coordinated to copper atom in Cu-Cys but cysteine was coordinated to copper via its thiol functional group [25].

Based on hard and soft acids and bases principle, when Cu-Cys complex was capped with GNPs, it seems that thiol group in cysteine shows greater tendency to Au relative to Cu since gold is softer than copper [29]. Consequently, by chemisorption of GNPs on Cu-Cys complex, GNPs/Cu-Cys nanocomposite was formed. But in view of the fact that Cu-S and Au-S bands are not active in the normal FT-IR range (Fig. 1a), Raman spectroscopy was carried out to confirm the existence of Cu-S and more details about replacement of copper atoms with Au.

As seen in Fig. 1b the disappearance of S-H stretching at 2546 cm^{-1}, a prominent Raman absorption peak, could be a sign for the formation of a covalent bound between sulfur and Cu or Au in Cu-Cys or GNPs/Cu-Cys, respectively [30, 31]. In the low-wavenumber region of Fig. 1, C-S stretching modes appeared in the range from 570 to 750 cm^{-1} [32, 33] and the Cu-S stretching vibration in Cu-Cys (solid line) was appeared at 370 cm^{-1} [31]. While, in GNPs/Cu-Cys nanocomposite (dotted line), not only the C-S stretching vibration shifted to higher frequencies but also, a new peak was appeared at 450 cm^{-1} which might be attributed to the formation

Table 1 The analytical parameters of six carbon paste electrodes containing different amount of Cu-Cys complex toward $O_2^{\bullet-}$

Electrode no.	Cu-Cys complex (mg)	Graphite powder (mg)	Paraffin oil (mg)	Linear range (μM)	Detection limit (μM)	Sensitivity ($\mu A.\mu M^{-1}.cm^2$)
1	–	20	15	–	–	–
2	1	20	15	20–77	4.8	0.016
3	2	20	15	20–95	4.6	0.016
4	3	20	15	20–95	2.5	0.028
5	4	20	15	10–130	2.2	0.041
6	5	20	15	10–77	2.0	0.041

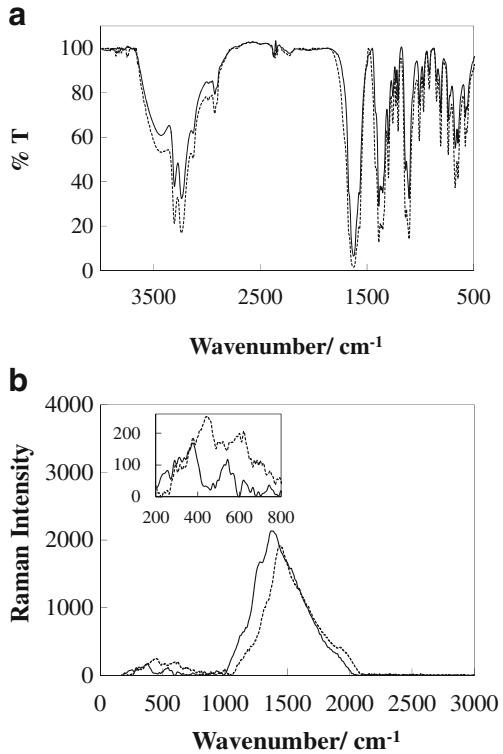

Fig. 1 FT-IR absorption spectra (**a**) and Raman spectra (**b**) of Cu-Cys complex (*solid line*) and GNPs/Cu-Cys nanocomposite (*dotted line line*) . The insert shows a magnified part of the spectra in the low-wavenumber region

of Au-S [34]. Additionally, according to literature [30], the different modes of NH_3^+ vibrations (rocking and asymmetric bending) in the wave number from 1000 to 1600 cm^{-1} represent the dipolar ionic (zwitterions) form of Cys. So, the appearance of a strong band at 1368 cm^{-1} in Cu-Cys (solid line) may be due to the combination of different modes of NH_3^+ vibrations into a single mode. However, by formation of GNPs/Cu-Cys nanocomposite, this band shifted to 1435 cm^{-1} (dotted line). This shift (67 cm^{-1}) could be due to the formation of a new coordination (either N-Au or N-Cu).

For measuring the average sizes of GNPs and GNPs/Cu-Cys nanocomposite, DLS technique was used. The results showed that the average diameter for diluted GNPs, Cu-Cys complex and GNPs/Cu-Cys nanocomposite in deionized water were 18.8, 151.7 and 77.0 nm respectively. These DLS data not only indicated that Cu-Cys capped on GNPs, but also a new nano compound formed.

The formation of the GNPs/Cu-Cys nanocomposite was also confirmed by studying two and three dimensional AFM images. The AFM images for Cu-Cys, GNPs and GNPs/Cu-Cys, at glass plate, are shown in Fig. S1 (Electronic Supplementary Material). Comparison of the rough morphology of Cu-Cys complex, GNPs and GNPs/Cu-Cys nanocomposite revealed that GNPs are uniformly distributed on the Cu-Cys surface (Fig. S1 A, B and C).

SOD mimetic activity of GNPs/Cu-Cys nanocomposite

The SOD mimetic activity of Cu-Cys and GNPs/Cu-Cys nanocomposite and also their related individual components such as, copper(II) acetate, Cys and GNPs were determined by using the pyrogallol autoxidation inhibition assay [27]. The results in term of IC_{50} values were compared with the activity obtained by the native Cu, Zn SOD and reported in Table 2.

The IC_{50} values of compounds indicate that all individual components related to GNPs/Cu-Cys nanocomposite exhibited SOD mimic activity. As seen, by coordinating copper(II) acetate to Cys in Cu-Cys complex SOD mimic activity rises 4 times. Additionally, GNPs, conjugated to Cu-Cys complex in GNPs/Cu-Cys nanocomposite, enhance SOD mimic activity of Cys in Cu-Cys complex more than 10 times. These data mention that a new and stable GNPs/Cu-Cys nanocomposite was formed since its SOD mimic activity is quite different from its starting components.

Suggested mechanism for superoxide dismutation of GNPs/Cu-Cys nanocomposite

As mentioned, copper-zinc SODs are most common in eukaryotic cells. The active center of this type of SODs consists of copper (II) and Zinc (II) ions. It has been proved that the copper ion plays the main role in the catalytic electron transfer, while, the role of zinc ion is to organize the structure of enzyme. And also, the active site of SOD consists of positive charged amino acid residues, including Lys-120, Lys-134, and Arg-141. Hence, the positive cavity of active site induces the electrostatic attraction and fixes $O_2^{\bullet-}$ in a favorable location to coordinate to copper(II). In this sense, Cu(II)-Cu(I) cycle carries out the catalysis of superoxide dismutation. The reactions are as follows [35]:

$$Cu^{2+} + O_2^{cdot-} \xrightarrow{SOD} O_2 + Cu^{+}$$
$$O_2^{cdot-} + Cu^{+} + 2H^{+} \rightarrow H_2O_2 + Cu^{2+}$$

As it was concluded in previous section, GNPs/Cu-Cys nanocomposite shows SOD mimetic activity in scavenging $O_2^{\bullet-}$. Because, it is composed up three convenient ingredients

Table 2 Comparison between the activity of the native SOD with those obtained by copper complexes and other related compounds

Compound	IC_{50}[a] ($\mu g.mL^{-1}$)
Cys	60
$Cu(CH_3COO)_2$	16
GNPs	10
Cu-Cys	4.1
GNPs/Cu-Cys	0.3
Native SOD[b]	0.1

[a] For IC_{50} definition see text

[b] Taken from [27]

for scavenging $O_2^{\bullet-}$ such as copper (II), cysteine and GNPs. Firstly, copper (II) in GNPs/Cu-Cys nanocomposite play a key role in catalysis the $O_2^{\bullet-}$ dismutation as the same as above reaction occurs in native SOD. Secondly, cysteine amino acid is a good material in $O_2^{\bullet-}$ dismutation. As, it was reported that thiol groups which ended by amine or hydroxyl may efficiently oxidizes $O_2^{\bullet-}$ [36] and cysteine contains thiol, amine and hydroxyl. And finally, GNPs can efficiently catalyze the dismutation of $O_2^{\bullet-}$ by adsorbing and electron transferring of $O_2^{\bullet-}$ to GNPs [23, 20, 19]. Consequently, based on above reasons and our previous findings we prepared Cu-Cys complex as it shown in Fig. 2. GNPs capped on it and GNPs/Cu-Cys nanocomposite for enhancing superoxide dismutation of Cu-Cys complex. At that moment the copper and GNPs complete the electron transferring and dismutation of superoxide via catalytic redox cycle. Based on Raman data, when GNPs/Cu-Cys nanocomposite formed from Cu-Cys complex the same absorption peaks presented but two distinct changes occurred, first appearing new Au-S bond and the other a little shifting in NH_3^+ absorption peak. So, we can conclude that although the S-atom in Cu-S bond is broken and new Au-S bond formed, there are some Cu-S bonds in GNPs/Cu-Cys nanocomposite. Furthermore, the absorption shift in NH_3^+ presented the amine group of cysteine in Cu-Cys complex self-assembled on GNPs a little. So, in this way a positive cavity for trapping $O_2^{\bullet-}$ formed as comparable with native SOD. As a result, the colloidal nature (extremely high surface area) of the GNPS which cause enhancing electron transfer, it's known SOD mimic activity, producing positive cavity for adsorbing $O_2^{\bullet-}$ and the catalytic activity of Cu-Cys complex can be synergistically exploited.

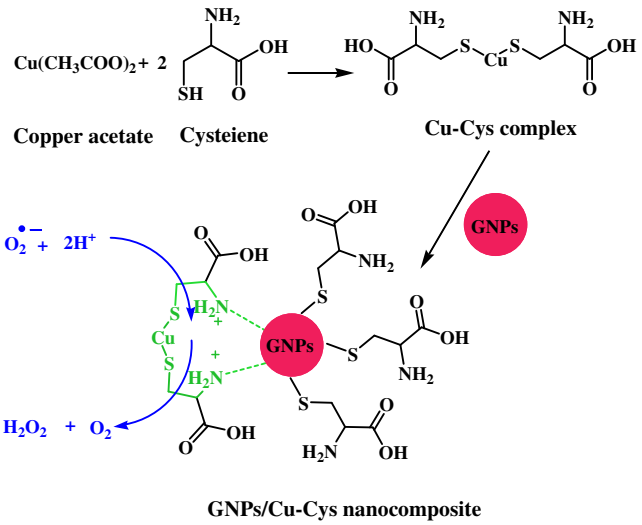

Fig. 2 Process for the synthesis of GNPs/Cu-Cys nanocomposite and suggested mechanism for $O_2^{\bullet-}$ scavenging

Cyclic voltammetry and electrochemical impedance spectroscopy

To evaluate the electrons transferring ability of different modified electrodes, cyclic voltammetry was used. The cyclic voltammograms (CVs) of different modified electrodes in $K_3Fe(CN)_6$ at the scan rate of 0.1 Vs^{-1} were recorded. As seen in Fig. 3a (Curve a) a pair of well-defined redox peaks for Fe^{III}/Fe^{II} was observed at naked CP electrode. By modification of CP electrode with Cu-Cys complex, both the peak height and peak separation were reduced (Curve b). Reducing the peak height could mainly be due the resistance of Cys and enhancing the electron transfer could perhaps be due to the catalytic activity of Cu-Cys. By adsorbing GNPs on either bare CP (Curve c) or Cu-Cys/CP (Curve d), the current strongly increased regarding the role of GNPs in electron transfer mediation between Cu-Cys and the CP electrode. Comparing the current height and peak separation of Cu-Cys/CP (Curve b) and GNPs/Cu-Cys/CP (Curve d) revealed that the nanocomposite provided much more catalytic activity than Cu-Cys complex. The value of formal potential [E^0=(Epc+Epa)/2] for Cu-Cys/CP and GNPs/Cu-Cys/CP were measured to be 0.24 and 0.30, respectively. Also the

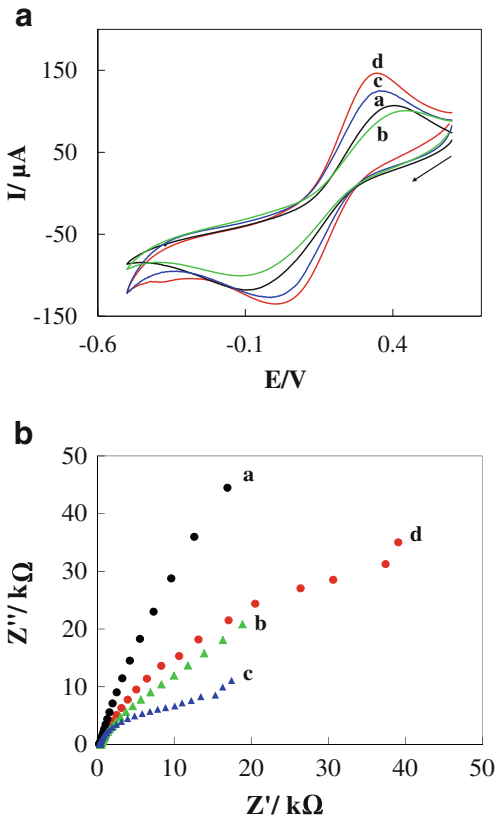

Fig. 3 **a** Comparison between the electron transferring abilities of different modified CP electrodes and **b** Normalized electrochemical impedance spectroscopy. The letters (a) to (d) stand for CP, Cu-Cys/CP, GNPs/CP and GNPs/Cu-Cys/CP, respectively

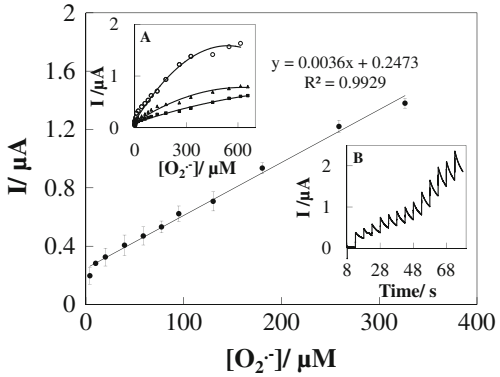

Fig. 4 Calibration curve for determination of $O_2^{\bullet-}$ using GNPs/Cu-Cys/CP. In inset (A) the amperometric responses of three modified electrodes (GNPs/Cu-Cys/CP (○), Cu-Cys/CP (●) and GNPs/CP (▲)) toward $O_2^{\bullet-}$ were compared. In inset (B) the amperometric responses of the GNPs/Cu-Cys/CP toward successive addition of $O_2^{\bullet-}$ was shown. The measurements were carried out in a cell containing 3 mL potassium phosphate buffer (0.02 M, pH 7.4) at 0.25 V vs Ag/AgCl and each point shows the average of three experiments

value of the peak separation for Cu-Cys/CP and GNPs/Cu-Cys/CP were 0.32 and 0.29 V, respectively. These data again emphasize the superiority of nanocomposite related to the complex.

Electrochemical impedance spectroscopy (EIS) was used to investigate the electrodes/solution interface properties. It provides useful information through the electrode surface modification process. EIS of different modified electrodes in $K_3Fe(CN)_6$ (5 mM)/KCl (50 mM) were recorded. The results of different modified electrodes in the frequency range from 102 to 105 Hz are presented as Nyquist plots (-Z" vs. Z') in Fig. 3b.

As shown, the CP plot showed the maximum charge transfer resistance and minimum conductivity. The resistance of the CP (Curve a) is more than that of the GNPs/CP (Curve b). Comparing Curve a with Curve b illustrated that the GNPs was obviously able to decrease the interfacial electron transfer resistance at the carbon pate electrode surface. In the next experiments, when Cu-Cys complex was placed in the carbon paste (Curve c), the EIS of the resulting electrode showed an obvious semicircle domain with a diameter of about 40 kΩ. The semicircle diameter is a criterion corresponding to the electron-transfer resistance. But, the presence of the GNPs on Cu-Cys complex in GNPs/Cu-Cys/ CP could decrease the resistance to 15 kΩ (Curve d). This indicated that the Cu-Cys complex molecules could result in more charge transfer resistance on electrode surface because of; the presence of cysteine amino acid in CP. But, the GNPs were obviously able to reestablish the electron transfer pathway at the sensing interface due to the conductive nature of GNPs. Comparison of Curves b and d reveals that the GNPs were obviously attached to complex not just to carbon paste surface because; the resistance in GNPs/Cu-Cys/CP is much lower than GNPs/CP. And also we declare that, the attachment of GNPs to Cu-Cys complex is through thiol group of cysteine so; GNPs subsequently substituted some copper ions in Cu-Cys complex.

SOD mimic electrochemical activity

Amperometry was used for determining SOD mimic electrochemical activity of Cu-Cys complex, GNPs and GNPs/Cu-Cys nanocomposite. The electrode response toward $O_2^{\bullet-}$ was monitored on CP electrodes containing Cu-Cys complex, free GNPs and GNPs/Cu-Cys nanocomposite. It is well known that the analytical characteristics of the CP electrodes depend significantly on the paste composition [36]. Thus, at first the response of the Cu-Cys ingredient in the presence of constant amount of graphite powder toward $O_2^{\bullet-}$ was investigated (Table 1).

The results indicate that the best detection limit was obtained for electrodes No. 5 and 6 while linear range for electrode No. 5 was wider. Therefore, the combination ratio of electrode No. 5 contains 4 mg Cu-Cys complex was chosen for preparation of subsequent GNPs/Cu-Cys/CP, Cu-Cys/CP and GNPs/CP electrodes. Figure 4 (inset A) represent the comparison between the response of different modified carbon paste electrodes toward $O_2^{\bullet-}$. Also, the value of different analytical parameters was presented in Table 3. As seen, the amperometric response (SOD mimic activity) of different modified electrodes toward $O_2^{\bullet-}$ improved in the following order: GNPs/Cu-Cys/CP > Cu-Cys/CP > GNPs/CP. As discussed in the suggested mechanism GNPs, due to its catalytic activity, is able to dismutate $O_2^{\bullet-}$. However by applying Cu-Cys complexs, the dismutation of $O_2^{\bullet-}$ is improved due to the redox property of both Cu(II) and thiol groups in cysteine [36]. On the other hand, GNPs beside Cu-Cys complex forms

Table 3 Comparison between the responses of different modified carbon paste electrodes toward $O_2^{\bullet-}$

Electrode	Complex (mg)	Graphite powder (mg)	Paraffin oil (mg)	Linear range (µM)	Detection limit (µM)	Sensitivity (µA. $\mu M^{-1}.cm^{-2}$)
GNPs/CP	0	20	15	20– 130	13	0.024
Cu-Cys/CP	4	20	15	10– 130	2.2	0.041
GNPs/Cu-Cys/CP	4	20	15	3.1– 326	0.2	0.073

CP Carbon paste electrode, *GNPs* Gold nanoparticles, *Cu-Cys* Copper cysteine complex

Table 4 Comparison between the analytical parameters obtained by GNPs/CuCys/CP electrode and those attained by different modified electrodes reported in the literature

Materials	Methods	Linear range (μM)	Detection limit (μM)	Sensitivity ($\mu A.\mu M^{1}.cm^{-2}$)	Selectivity to $O_2^{\bullet-}$ over H_2O_2 (%)	Ref.
Mn-CSalen-HSMs	Chemiluminescence	$320–754\times10^2$	100	–	–	[6]
MnTMPyP-PPy/Pt	Electrochemistry	0.6–1000	0.60	0.12	–	[38]
MWCNTs/$Mn_2P_2O_7$–formylstyrylpyridine/GCE	Electrochemistry	0.08–3.19 and 3.67 −11.65	0.03	–	good	[39]
PDDA/MWCNTs–Pt/GCE	Electrochemistry	0.7–300	0.10	0.86	–	[40]
GNPs/Cu-Cys/CP	Electrochemistry	3.1–326	0.25	0.07	good	This work

SiC silicon carbide nanoparticles, *Mn-CSalen* Mn-bis(salicylaldehyde)-3,4-Diaminobenzoic acid, *HSMs* hollow silica microspheres, *MnTMPyP* manganese(III) tetrakis(1-methyl-4-pyridyl) porphyrin, *PPy* polypyrrole, $Mn_2P_2O_7$ manganous pyrophosphate, *MWCNTs* multiwalled carbon nanotubes, *PDDA* poly-diallyldimethylammonium chloride, *Pt* Pt nanoparticles, *GC* glassy carbon

a nanocomposite which improves the electron transferring ability and also creates a positive cavity for adsorbing $O_2^{\bullet-}$. These all together, enhances the particular catalytic activity for $O_2^{\bullet-}$ dismutation.

Calibration curve for $O_2^{\bullet-}$ measurement

For determination of $O_2^{\bullet-}$ concentration amperometric method was used. Using GNPs/Cu-Cys/CP electrode a typical amperometric response for $O_2^{\bullet-}$ measurement was obtained (Fig. 4, inset B). Based on the data obtained by amperometric measurement of $O_2^{\bullet-}$ standard samples a calibration curve was plotted (Fig. 4). As seen the amperometric response of GNPs/Cu-Cys/CP electrode was linear in the $O_2^{\bullet-}$ concentration range from 3.1 to 326 μM. The linear regression equation of the current versus $O_2^{\bullet-}$ concentration was I (μA)=0.0036 [$O_2^{\bullet-}$] (μM) +0.2473 (R=0.9929, n=3). The current sensitivity was obtained to be 0.073 A M^{-1} cm^{-2}. The detection limit (DL) at signal to noise ratio of 3 (S/N=3) was calculated according to the Eq. 1:

$$DL = 3.3\,\sigma/S \quad (1)$$

Where, σ is standard deviation of the response and S is the slope of calibration curve [37]. The relative standard deviation of the GNPs/Cu-Cys/CP electrode response at the concentration of 3.1 μM was 0.03 for three successive measurements. Based on Eq. 1, the detection limit was calculated to be as low as 0.25 μM, at S/N=3.

So far the biosensors developed for detection of $O_2^{\bullet-}$ has been mostly based on natural macromolecules such as superoxide dismutase and different cytochromes. However, these biosensors are restricted by their poor structural stability and high cost. These limitations could be narrowed by developing none-enzymatic $O_2^{\bullet-}$ sensors [6, 38–40]. Table 4 represents the comparison between the analytical parameters for $O_2^{\bullet-}$ sensor obtained by the present sensor and those attained by different modified none-enzymatic sensors reported in the literature. As seen, the sensitivity of two sensors was not reported. But the remaining two electrodes have relatively higher sensitivity. However, they did not report the selectivity for these electrodes probably due to the lack of selectivity. While, the results obtained by GNPs/CuCys/CP electrode show an excellent selectivity toward $O_2^{\bullet-}$. Moreover, the advantages such as simplicity of procedure for electrode preparation, low cost material for nanocomposite synthesis and lesser steps for the preparation of the sensor make its application more users friendly.

Specificity

The relative response of GNPs/Cu-Cys/CP electrode toward $O_2^{\bullet-}$ and common interferences is shown in Fig. 5. As observed, either pure DMSO or citric acid (CA), uric acid (UA) or H_2O_2 does not show significant response. But DMSO containing $O_2^{\bullet-}$ represents a significant amperometric

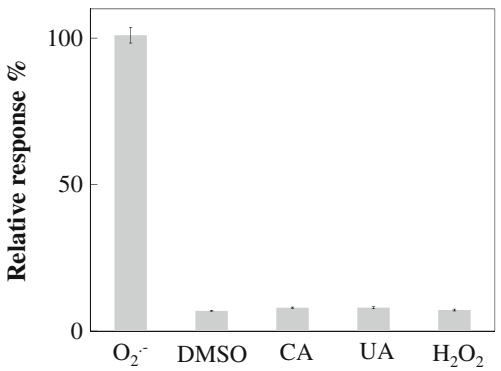

Fig. 5 The specificity of GNPs/Cu-Cys/CP electrode toward $O_2^{\bullet-}$. The amperometric measurements were carried out at 0.25 V vs Ag/AgCl in 3 mL potassium phosphate buffer (0.02 M, pH 7.4) while the concentration of each sample was 3 μM

response. Therefore, one may conclude that GNPs/Cu-Cys nanocomposite has a novel SOD mimic activity toward $O_2^{\bullet-}$.

Conclusions

The nanocomposite contained Cu-Cys complex and GNPs exhibited significant SOD mimic behavior. The combination of GNPs and Cu-Cys complex elevated the electrochemical signal toward $O_2^{\bullet-}$. Considering the role of individual components including thiol group in Cys, as $O_2^{\bullet-}$ oxidizer [36], copper ion as a prosthetic group in native SOD which catalyzes the electron transfer in $O_2^{\bullet-}$ dismutation [35], GNPs which accelerate electron transfer for $O_2^{\bullet-}$ dismutation [23, 20, 19], it seems that all these effects are appeared synergically by the nanocomposite. The biomimetic sensor which was developed by immobilization of this nanocomposite in a CP electrode has the advantages of simplicity, stability, reusability and cost effectiveness.

Acknowledgments Financial supports provided by the Research Council of the University of Tehran are gratefully appreciated.

References

1. Lee H, Park W, Lim D (2010) Synthesis and SOD activity of manganese complexes of substituted pyridino pentaaza macrocycles that contain axial auxiliary. Bioorg Med Chem Lett 20(8):2421–2424
2. Muscoli C, Cuzzocrea S, Riley DP, Zweier JL, Thiemermann C, Wang ZQ, Salvemini D (2003) On the selectivity of superoxide dismutase mimetics and its importance in pharmacological studies. Br J Pharmacol 140:445–460
3. Ge L, Ge S, Liu S, Yu J (2011) Synthesis of a novel rigid artificial superoxide dismutase based on modified hollow mesoporous silica microspheres. J Inorg Organomet Polym Mater 21(4):809–815
4. Batinić-Haberle I, Rebouças JS, Spasojević I (2010) Superoxide dismutase mimics: chemistry, pharmacology, and therapeutic potential. Antioxid Redox Signal 13(6):877–918
5. Riley DP (1999) Functional mimics of superoxide dismutase enzymes as therapeutic agents. Chem Rev 99(9):2573–2588
6. Yu J, Ge L, Liu S, Dai P, Ge S, Zheng W (2011) Facile and scalable synthesis of a novel rigid artificial superoxide dismutase based on modified hollow mesoporous silica microspheres. Biosens Bioelectron 26(5):1936–1941
7. Batinić-Haberle I, Liochev SI, Spasojević I, Fridovich I (1997) A potent superoxide dismutase mimic: manganese beta-octabromo-meso-tetrakis-(N-methylpyridinium-4-yl) porphyrin. Arch Biochem Biophys 343(2):225–233
8. Salvemini D, Wang Z-Q, Zweier JL, Samouilov A, Macarthur H, Misko TP, Currie MG, Cuzzocrea S, Sikorski JA, Riley DP (1999) A nonpeptidyl mimic of superoxide dismutase with therapeutic activity in rats. Science 286(5438):304–306
9. Miriyala S, Spasojevic I, Tovmasyan A, Salvemini D, Vujaskovic Z, St Clair D, Batinic-Haberle I (2012) Manganese superoxide dismutase, MnSOD and its mimics. Biochim Biophys Acta (BBA)-Mol Basis Dis 1822(5):794–814
10. Puterová Z, Valentová J, Bojková Z, Kožíšek J, Devínsky F (2011) Synthesis, crystal structure and antiradical effect of copper (II) Schiff base complexes containing five-, six-and unusual seven-membered rings. Dalton Trans 40(7):1484–1490
11. Patel RN, Singh A, Shukla KK, Patel DK, Sondhiya VP (2010) Copper (II) complexes with N-(2-hydroxyethyl)-2-iminodiacetic acid and imidazoles: crystal structure, spectroscopic studies and superoxide dismutase activity. Transit Met Chem 35(5):577–584
12. Gu Q, Le XY, Lin QB, Liao SR, Ma XD, Feng XL (2007) Synthesis, Characterization and SOD Activities of IP-copper (II)-L-amino Acid Complexes. Chin J Chem 25(6):791–796
13. Rafiee-Pour H-A, Ghourchian H, Eskandari K (2011) Cysteine function in superoxide dismutase direct electrochemistry and superoxide anion sensing. Anal Bioanal Electrochem 3(3):215–226
14. Korsvik C, Patil S, Seal S, Self WT (2007) Superoxide dismutase mimetic properties exhibited by vacancy engineered ceria nanoparticles. Chem Commun 10:1056–1058
15. Kajita M, Hikosaka K, Iitsuka M, Kanayama A, Toshima N, Miyamoto Y (2007) Platinum nanoparticle is a useful scavenger of superoxide anion and hydrogen peroxide. Free Radic Res 41(6):615–626
16. Kim J, Takahashi M, Shimizu T, Shirasawa T, Kajita M, Kanayama A, Miyamoto Y (2008) Effects of a potent antioxidant, platinum nanoparticle, on the lifespan of Caenorhabditis elegans. Mech Ageing Dev 129(6):322–331
17. Hamasaki T, Kashiwagi T, Imada T, Nakamichi N, Aramaki S, Toh K, Morisawa S, Shimakoshi H, Hisaeda Y, Shirahata S (2008) Kinetic analysis of superoxide anion radical-scavenging and hydroxyl radical-scavenging activities of platinum nanoparticles. Langmuir 24(14):7354–7364
18. JuanáLong Y, FangáLi Y, JiaáZheng J, ZhiáHuang C (2011) Visual observation of the mercury-stimulated peroxidase mimetic activity of gold nanoparticles. Chem Commun 47(43): 11939–11941
19. Hu X, Liu J, Hou S, Wen T, Liu W, Zhang K, He W, Ji Y, Ren H, Wang Q (2011) Research progress of nanoparticles as enzyme mimetics. Sci China Phys, Mech Astron 54(10):1749–1756
20. Pasquato L, Pengo P, Scrimin P (2004) Functional gold nanoparticles for recognition and catalysis. J Mater Chem 14(24):3481–3487
21. Villalonga R, Camacho C, Cao R, Hernández J, Matías JC (2007) Amperometric biosensor for xanthine with supramolecular architecture. Chem Commun 9:942–944
22. Baron R, Willner B, Willner I (2007) Biomolecule–nanoparticle hybrids as functional units for nanobiotechnology. Chem Commun 4:323–332
23. Cao R Jr, Villalonga R, Díaz-García AM, Cao R, Rojo T, Rodríguez-Argüelles MC (2011) Gold nanoparticles enhancing dismutation of superoxide radical by its bis (dithiocarbamato) copper (II) shell. Inorg Chem 50(11):4705–4712
24. Hyland K, Auclair C (1981) The formation of superoxide radical anions by a reaction between O2, OH-and dimethyl sulfoxide. Biochem Biophys Res Commun 102(1):531–537
25. Monan Ahmad MSI, Tahir N, Islam A (2011) Solvent free synthesis copper (II) cysteine complexes. World Appl Sci 14(2):210–214
26. Cooperá Stevenson P (1951) A study of the nucleation and growth processes in the synthesis of colloidal gold. Discuss Faraday Soc 11: 55–75
27. Marklund S, Marklund G (1974) Involvement of the superoxide anion radical in the autoxidation of pyrogallol and a convenient assay for superoxide dismutase. Eur J Biochem 47(3):469–474
28. Liz-Marzán LM (2006) Tailoring surface plasmons through the morphology and assembly of metal nanoparticles. Langmuir 22(1):32–41
29. Pearson RG (1963) Hard and soft acids and bases. J Am Chem Soc 85(22):3533–3539
30. Aryal S, BKC R, Dharmaraj N, Bhattarai N, Kim CH, Kim HY (2006) Spectroscopic identification of SAu interaction in cysteine

capped gold nanoparticles. Spectrochim Acta A Mol Biomol Spectrosc 63(1):160–163
31. Dooley D, Moog R, Liu M, Payne W, LeGall J (1988) Resonance Raman spectra of the copper-sulfur chromophores in achromobacter cycloclastes nitrite reductase. J Biol Chem 263(29):14625–14628
32. Venkataramanan M, Murty K, Pradeep T, Deepali W, Vijayamohanan K (2000) Metal Ion Reactivity with 1, 4-benzenedimethanethiol monolayers on gold. Langmuir 16(20):7673–7678
33. Socrates G, Socrates G (2001) Infrared and Raman characteristic group frequencies: tables and charts, vol 245. Wiley, Chichester
34. Varnholt B, Oulevey P, Luber S, Kumara C, Dass A, Burgi T (2014) Structural Information on the Au-S Interface of Thiolate-Protected Gold Clusters: A Raman Spectroscopy Study. J Phys Chem C
35. Liochev SI, Fridovich I (2010) Mechanism of the peroxidase activity of Cu, Zn superoxide dismutase. Free Radic Biol Med 48(12):1565–1569
36. Chen XJ, West AC, Cropek DM, Banta S (2008) Detection of the superoxide radical anion using various alkanethiol monolayers and immobilized cytochrome C. Anal Chem 80(24):9622–9629
37. Committee AM (1987) Recommendations for the definition, estimation and use of the detection limit. Analyst 112(2):199–204
38. Rajesh S, Sethy NK, Bhargava K, Ilavazhagan G, Singh SK, Karunakaran C (2011) Electrochemical sensor for simultaneous measurement of nitrite and superoxide anion radical using superoxide dismutase-mimetic manganese (III) tetrakis (1-methyl-4-pyridyl) porphyrin on polypyrrole matrix. Sens Lett 9(5):1682–1688
39. Yuan L, Liu S, Tu W, Zhang Z, Bao J, Dai Z (2014) Biomimetic Superoxide Dismutase Stabilized by Photopolymerization for Superoxide Anions Biosensing and Cell Monitoring. Anal Chem
40. Kim SK, Kim D, You J-M, Han HS, Jeon S (2012) Non-enzymatic superoxide anion radical sensor based on Pt nanoparticles covalently bonded to thiolated MWCNTs. Electrochim Acta 81:31–36